ISTITUTO NAZIONALE DI FISICA NUCLEARE
Laboratori Nazionali di Frascati

LNF-78/13(R)
8 Marzo 1978

P. Spillantini: A LARGE ACCEPTANCE TOROIDAL MAGNET FOR THE STUDY OF MANY-BODY FINAL STATES AT A STORAGE RING. PRESENT POSSIBILITIES AND CONCEIVABLE IMPROVEMENTS.

Servizio Documentazione
dei Laboratori Nazionali di Frascati
Cas. Postale 13 - Frascati (Roma)

INFN - Laboratori Nazionali di Frascati
Servizio Documentazione

LNF-78/13(R)
6 Marzo 1978

P. Spillantini: A LARGE ACCEPTANCE TOROIDAL MAGNET FOR THE STUDY OF MANY-BODY FINAL STATES AT A STORAGE RING. PRESENT POSSIBILITIES AND CONCEIVABLE IMPROVEMENTS.

In standard multibody counter experiments only a few energetic particles are identified and accurately measured ("trigger particles") while the remaining ones (up to 10-20 at ISR, or PEP and PETRA) are roughly measured to give the pattern of the event.

To obtain a reasonable efficiency for the detection of complete final states the pattern identification device must cover nearly the whole solid angle (Fig. 1). For instance at the ISR γ rays from π^0 decay are often used as trigger particles over a small solid angle, and are registred by a detector located behind the $\gtrsim 4\pi$ detector for charged particles[1].

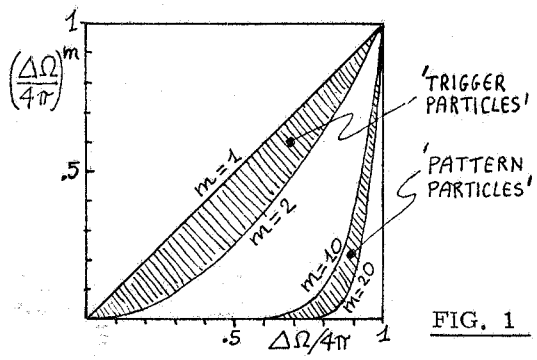

FIG. 1

Charged particles, in particular at low energy, may be too much disturbed by the pattern identification apparatus to be easily used as trigger particles. Moreover it is often desirable to generate a trigger depending on event pattern more than on the existence of a particular particle (e.g. large $p_\perp$ jets versus one large $p_\perp$ secondary). Therefore any effort should be made to perform complete particle identification and momentum measurement within the 4π detector. When this criterion is extended to the most energetic particles, the momentum becomes a very privileged kinematic variable, since resolutions and performancies of the detector are challenged for secondaries near the maximum energy of the machine and not at the most frequent energy of the products (which is often 10-20 times lower).

In such ambitious detectors, despite their complication and enormous cost, the request of complete particle identification inevitably implies some loss of solid angle for tracking. In addition, the request of momentum measurement for energetic secondaries makes the analysis of the detected events very complex, because low energy particles spiralize in strong or/and large volume magnetic fields, and describe a complex trajectory[2]. In such a situation the calculation of the efficiencies is difficult and can be strongly "model dependent".

A tentative solution of the above problems is to design large solid angle devices based on a lumped coil or a thin coil solenoid, in order to let a large fraction of the secondaries come out of the magnet and be available for additional measurements. However, the average transparency (including photons) cannot be very good (e.g. in a solenoid, the coil thickness is in general $\gtrsim 0.5$ radiation lengths), and also the difficulties of analysis mentioned are still present. Moreover the return yoke of the magnet must be integrated in the external device and causes limitations to its performances.

In the following we will describe a full solid angle device based on a magnetic field which is particularly suitable for pattern identification of a multibody event.

In scattering experiments "nature works in polar coordinates" (ϑ, φ; see Fig. 2) so that ideally the structure of the detector should be such that the various relevant measurements which are performed sequentially do not mix ϑ and φ. It is well known that as far as momentum measurement is concerned this can be obtained only analysing the produced particles in a toroidal magnetic field[3] generated by an electric current running along the beam axis ($B(\text{Tesla}) = 0.2 \frac{I(\text{MA})}{R(\text{m})}$). In this case the field lines are circles centered on the beam line (Fig. 3), and each particle moves on a bi-dimensional trajectory on a φ = const. plane (see Fig. 4). Hence the φ-pattern of the event is conserved; this should result into an important

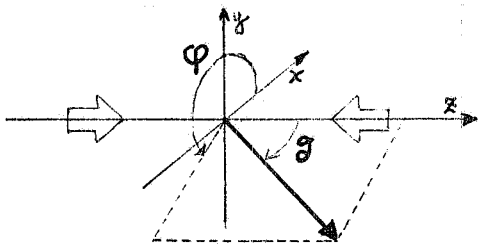

FIG. 2

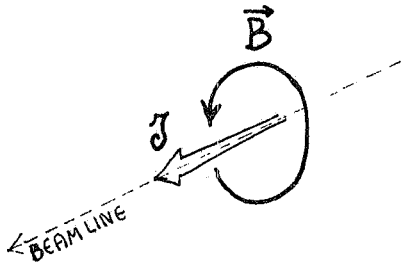

FIG. 3

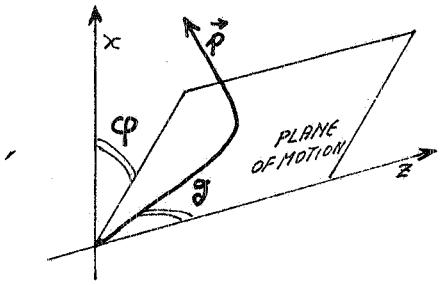

FIG. 4 - In a toroidal field each particles emerging from the beam line moves on a bi-dimensional trajectory on a φ = const. plane.

simplification of pattern recognition and momentum measurement. Furthermore the field lines are closed on themselves, and no iron is necessary to return the field flux, so that the space around the coil is completely free. For instance a toroidal coil can be used as internal core of other magnetic devices (see Fig. 5).

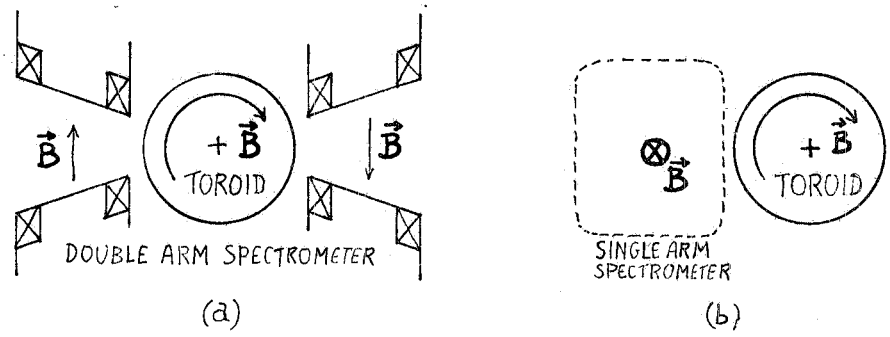

FIG. 5 - Since no iron is necessary to return the field flux a toroidal coil can be used as internal core of other magnetic devices.

In a toroid around the intersection of a storage ring, in order to produce the field a current must run in practice in a cylinder around the beam axis and parallel to it (Fig. 6). This is the main difficulty connected with the construction and implementation of a toroidal coil, as the current must be huge in order to produce a useful field, while the conductor carrying it must be very thin such as to be sufficiently transparent to the particles.

We shall now make a specific example. Consider an aluminium water-cooled coil covering the central region of a storage ring intersection, with a zenithal acceptance $\Delta\vartheta = 25^\circ - 155^\circ$, and

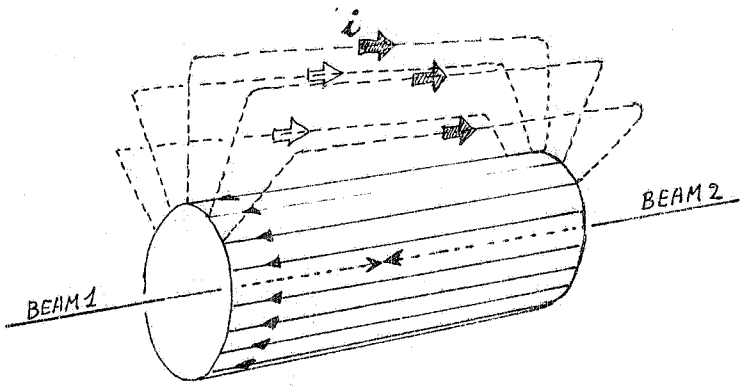

FIG. 6

two $\Delta\vartheta = 0^\circ - 20^\circ$ cones kept free along the beam (see Fig. 7a and footnote 1). Radially the device will have the structure and the dimensions reported in Fig. 7b.

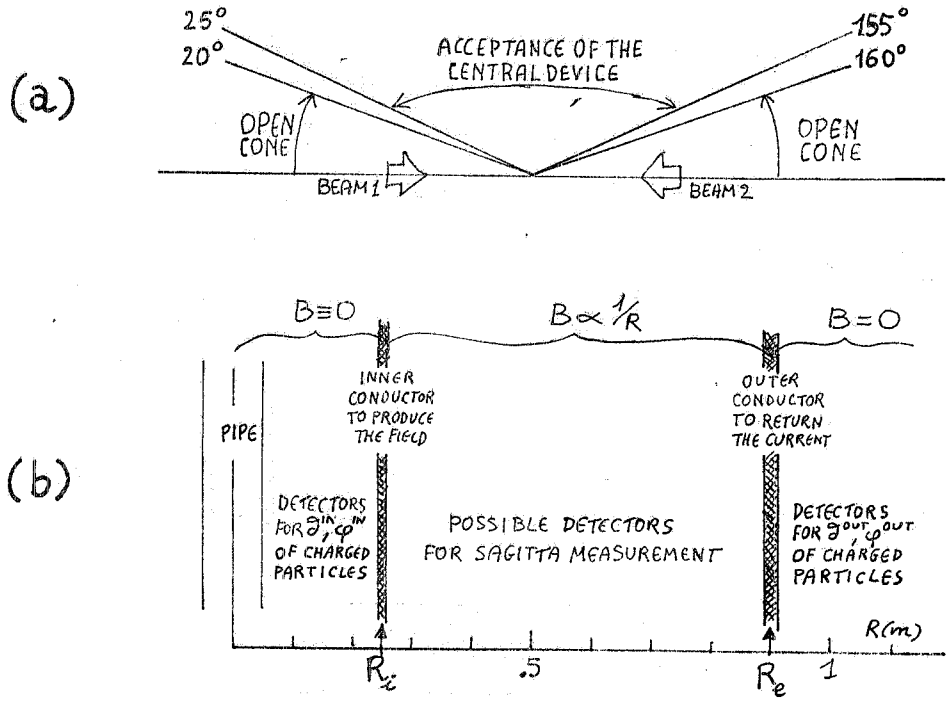

FIG. 7 - (a) Acceptance of the central toroid ($\Delta\Omega/4\pi = 0.91$) with indicated small angle cones free for any other device. The "blind region" amount to only $\sim 3\%$ of the total solid angle. (b) Radial structure of the central device.

In the design of the coil a fundamental choice must be made: the conductor producing the field (inner conductor) has to be "continuous". In fact lumped coil schemes (e.g. the Oktupus project[5] for DORIS) do not allow to cover a solid angle larger than $\simeq (0.6 \div 0.7) \times 4\pi$. Moreover the field inside the conductor is much stronger than outside (by about 2 in the Oktupus project) and the stresses between the coils are huge. On the other hand, for a continuous conductor the stresses between the coils can be well compensated and remains only a magnetic pressure which tends to expand the conductor radially. In practice, if the inner conductor is an aluminium water-cooled cylinder it can ea-

Note 1 - The use of toroids for momentum analysis in the small angle regions causes less problems and is not discussed here. There are already examples of such magnets either under construction or in operation[4].

sily resist the magnetic pressure (see Fig. 8). The outer conductor needed to return the current can be made either continuous or lumped, since the magnetic stresses at large radii are much weaker.

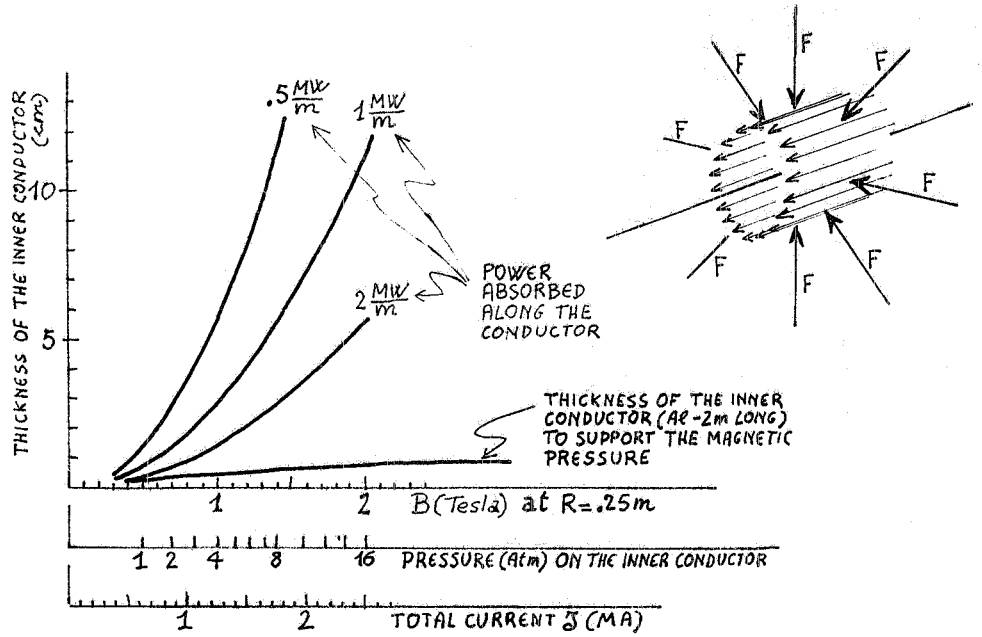

FIG. 8 - Thickness of the inner conductor as a function of the total carried current I, for some values of the electric power spent on it, compared with the thickness necessary to support the magnetic pressure on the conductor itself produced by I. The insert visualises the symmetry of the magnetic pressure on the inner conductor.

An aluminium water-cooled toroidal coil for the central region. -

The following is a tentative design of a realistic toroidal coil for a central magnetic detector.

We suggest that the coil be built by winding a conductor of different section in the different portions of the turn (see Fig. 9).

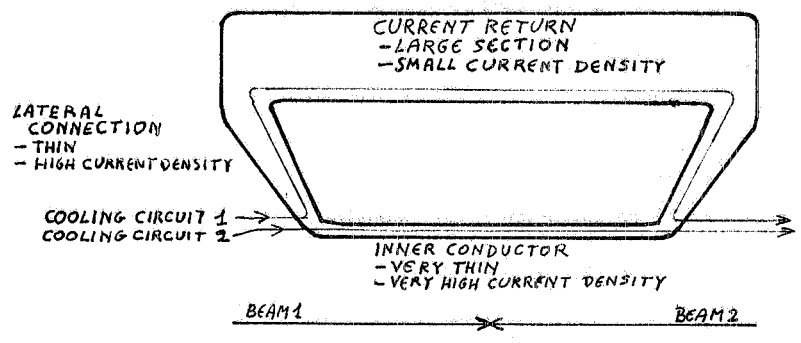

FIG. 9

Let 's' be the thickness of the inner conductor, and suppose that the section of the lateral and external conductors scale as s. We have:

$$R_{Total} = R_{Inner}(1+\varepsilon) \propto \frac{1}{s}$$

R_{Total} = electric resistance of the whole coil

R_{inner} = electric resistance of the inner conductor

$$I = \sqrt{\frac{P_{Total}}{R_{Inner}(1+\varepsilon)}} \propto \sqrt{s} \qquad \delta_{Max} \simeq \frac{I}{2\pi R_i s} \propto \frac{1}{\sqrt{s}}$$

P_{Total} = power dissipated in the whole coil
I = electric current
δ = density of current
R_i = radius of inner cylinder
$\varepsilon \lesssim 1$.

and in addition:

Multiple scattering in the inner conductor $\propto \sqrt{s}$

$\Delta\vartheta$ = deflection
X = sagitta
H_e = lateral displacement caused by the field

$\propto I \propto \sqrt{s}$

→ percent error due to multiple scattering INDEPENDENT of s

→ percent measurement errors $\propto 1/\sqrt{s}$.

It is therefore convenient to reduce the thickness s (i.e. to increase the transparency) as much as possible to reduce the overall measurement errors (notice however that the error caused by multiple scattering on the most important parameters - $\Delta\vartheta$ and H_e - does not depend on s). Therefore the current density in the material which cannot be increased indefinitely, represents the limiting factor to the transparency of the coil for a given required field.

As a reasonable guess we suppose to be able to run in the inner conductor a current density of ~ 50 A/mm^2 (less than 1/2 of the current density at which the CERN septum magnets are operated). Possibly an independent cooling circuit for this high current density section should be emploied (see again Fig. 9). With a power supply of 3 MW applied to a coil as sketched in Fig. 10, about 1/2 of the power is spent in the inner conductor, whose thickness would be 10 mm (footnote 2).

Charged hadrons have a $\sim 3\%$ probability to undergo an inelastic nuclear interaction in the inner conductor (estimated by averaging an isotropic distribution over the acceptance). Hence at the average charged particle multiplicities at the ISR or foreseen at PEP and PETRA energies ($\sim$6-8 charged prongs per event) only one charged particle in 5-7 events would be lost for momentum measurement, which looks very good even if momentum analysis of all charged secondaries is emphasized. The relevant parameters of the coil of Fig. 10 are quoted in Table I, and the corresponding resolutions are shown in Fig. 11.

TABLE I

Relevant parameters of the aluminium water-cooled coil sketched in Fig. 10

Overall dimensions :	Length (L)	2 m
	Max. Radius	1 m
	Min. Radius (R_i)	0.25 m
Solid angle fraction ($\Delta\Omega/4\pi$)		0.91
Inner conductor average thickness ($\langle s \rangle$)		1 cm
Power supply (P)		3 MW
Max magnetic field	(at R = 0.25 m)	0.65 T
Max magnetic pressure	(at R = 0.25 m)	1.65 atm
Max current density	(at R = 0.25 m)	52 A/mm^2
Total weight		0.36 t

Note 2 - The quantity, velocity and pressure of the water necessary to exchange this huge power released in such a small cylinder can be determined only in a detailed project. Values more conservative than those reported in the appendix can be obtained for the coils discussed here and in the following.

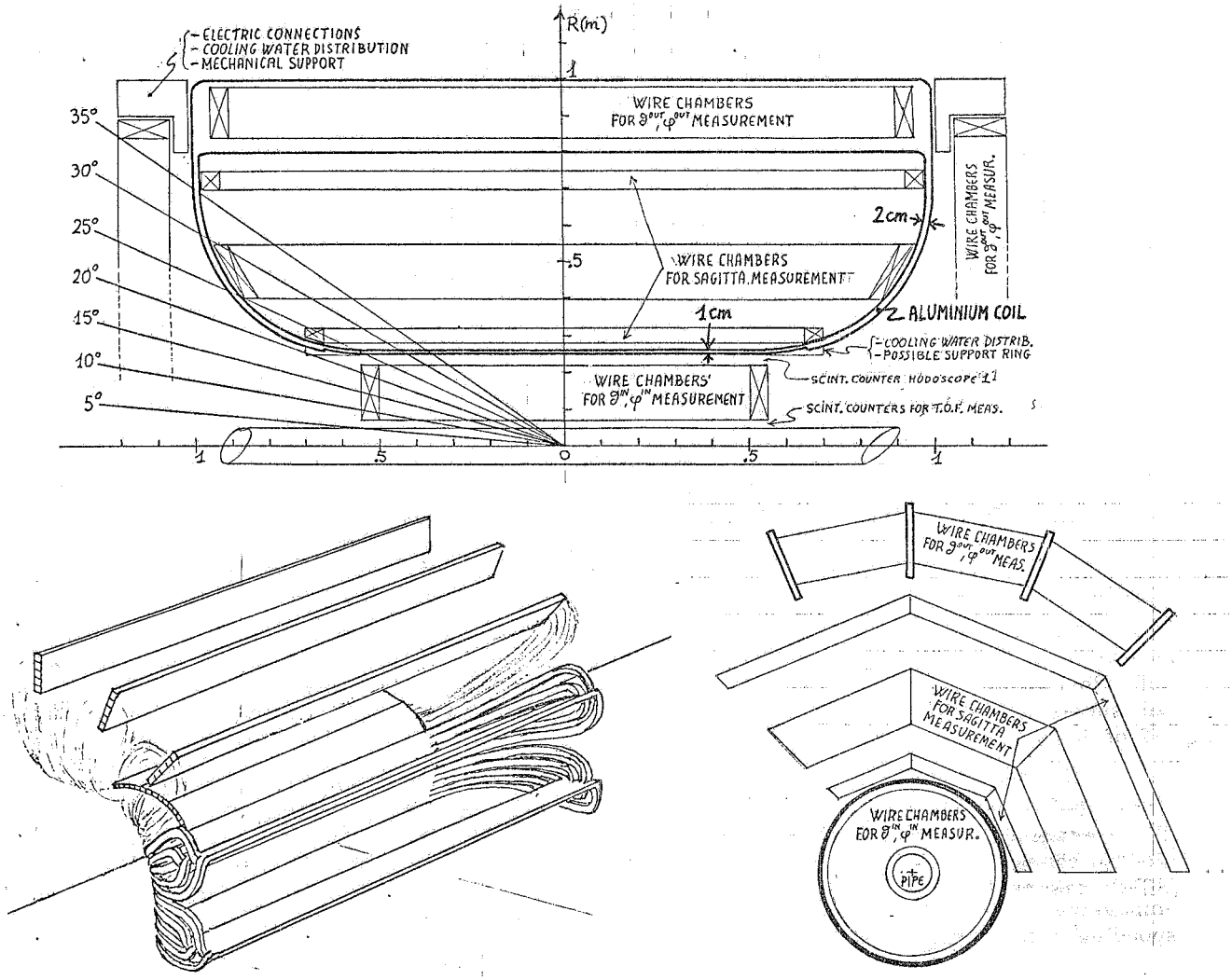

FIG. 10

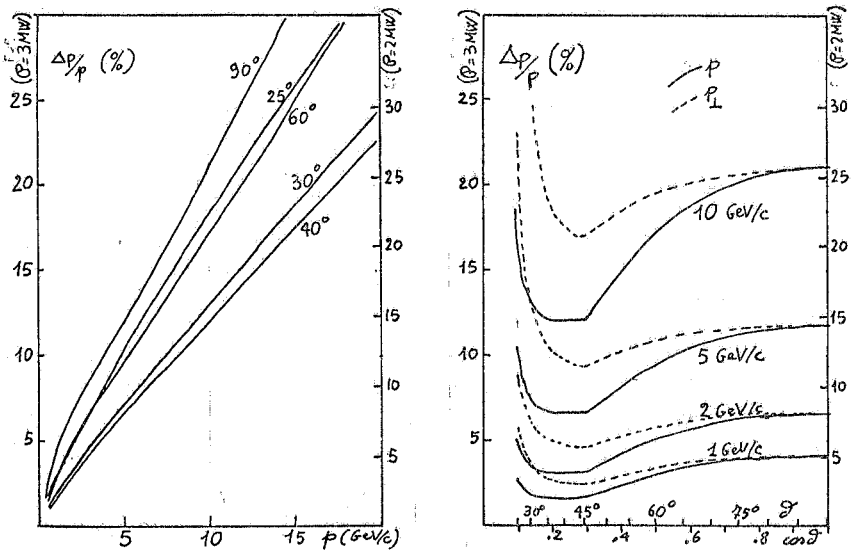

FIG. 11 - Momentum resolution for the coil of the Fig. 10 and Table I assuming a $\pm$0.2 mm error in the sagitta and a $\pm$1.4 mrad error (by 4 points at $\pm$0.2 mm) in the determination of ϑ.

To safe electric power the side and outer part of the coil can have a large cross section. If they are doubled while keeping the same current density in the inner conductor and thus the same momentum resolution, one would reduce the power to 2 MW.

A coil of optimum transparency. -

If a current density of $\sim$100 A/mm^2 is accepted in the inner conductor (see footnote 2) its thickness can be reduced to 4 mm (see Fig. 12). The coil would be the same as in Fig. 10 (except the inner conductor thickness) and the regime power still be 3 MW. The inner conductor can still resist the magnetic pressure (read again Fig. 8, with 1.67 MW/m dissipated in the inner conductor). The inelastic scattering probability would drop to 1.2% (e.g. one interaction each 11-14 events of PETRA-PEP) at the small price of a worsening by a factor of 1.33 of the magnetic field, and hence of all measurement errors (e.g. about 95% of the charged particles would have the momentum measured to better than 10%, at PEP and PETRA, and better than 4% at ISR).

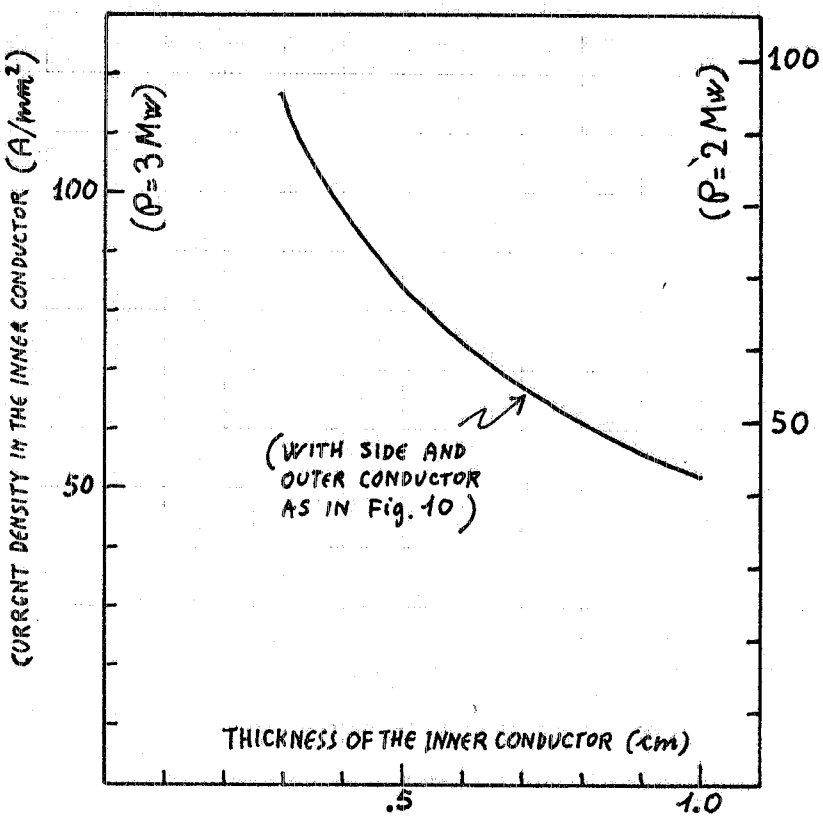

FIG. 12

Limiting momentum resolution: aluminium water-cooled coil. -

We would like to add here a few comments to the scheme suggested for PETRA[6] and reproduced in Fig. 13. The increase by a factor of 3 of the inner conductor thickness respect to Fig. 10 allows to improve the resolution (for the same 3MW power supply) only by $\sim$1.3 (pay attention to the different geometry; see footnote 3), while in average in about 50% of the events at least one charged particle would undergo an inelastic scattering in the inner conductor: this would produce some confusion in the

Note 3 - To take into account the different geometry of the two coils the resolution quoted in Fig. 13 must be reduced by $\sim$ 1.4 to be compared with those reported in Fig. 11.

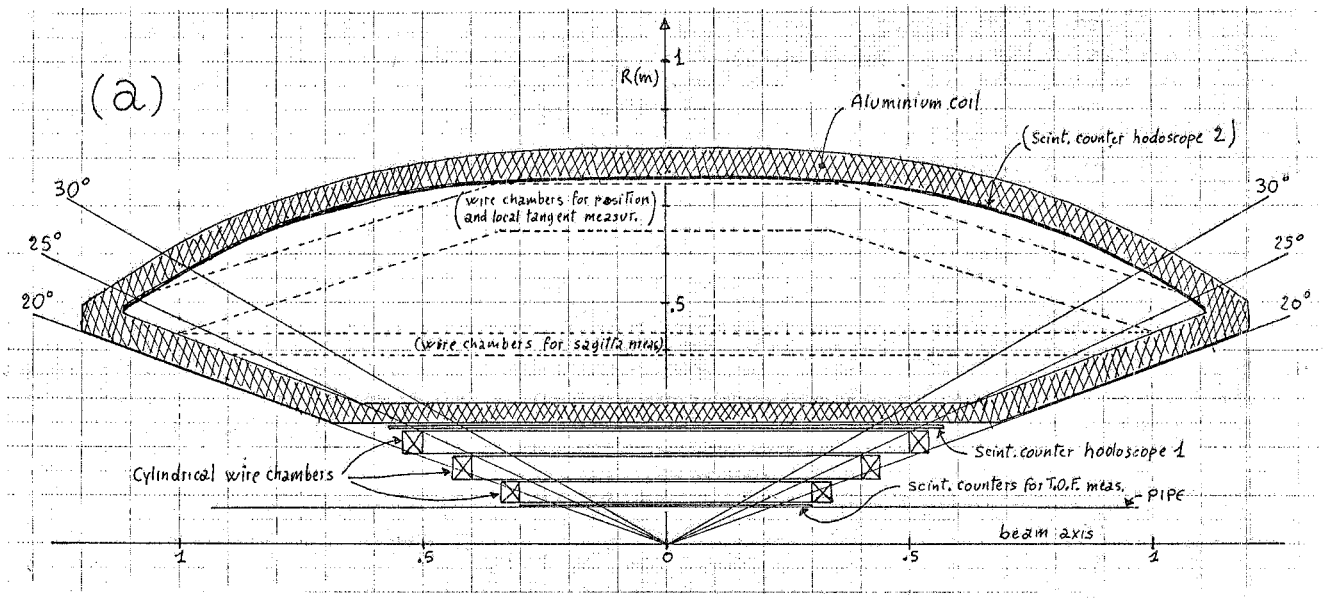

USUAL ALUMINIUM COIL

Overall dimensions: Length	2.4 m			
Max. R.	0.82 m			
Min. R.	0.25 m			
Solid angle fraction ($\Delta\Omega/4\pi$)	0.91			
Inner part thickness = 3 cm Al	(0.08 Labs)			
Outer part thickness = 5 cm Al	(0.13 Labs)			
Outer part shape:	'continuous'		'open fan'	
with power	1MW	2MW	1MW	2MW
Max. magn. field (Kgauss)	6.7	9.5	5.7	8.1
Max. pressure (Atm)	1.8	3.6	1.3	2.6
Max. current density (MAm^{-2})	18	25	15	21
Momentum resol. at p = 5 GeV/c				
$\theta = 90^{\circ}$	0.22	0.16	0.24	0.17
$\theta = 30^{\circ}$	0.14	0.10	0.16	0.11
Weight (tons)	2.1		1.1	

- It should be possible to open the coil in some distinct azimuthal sectors, complete of their detectors, so:

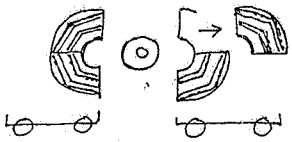

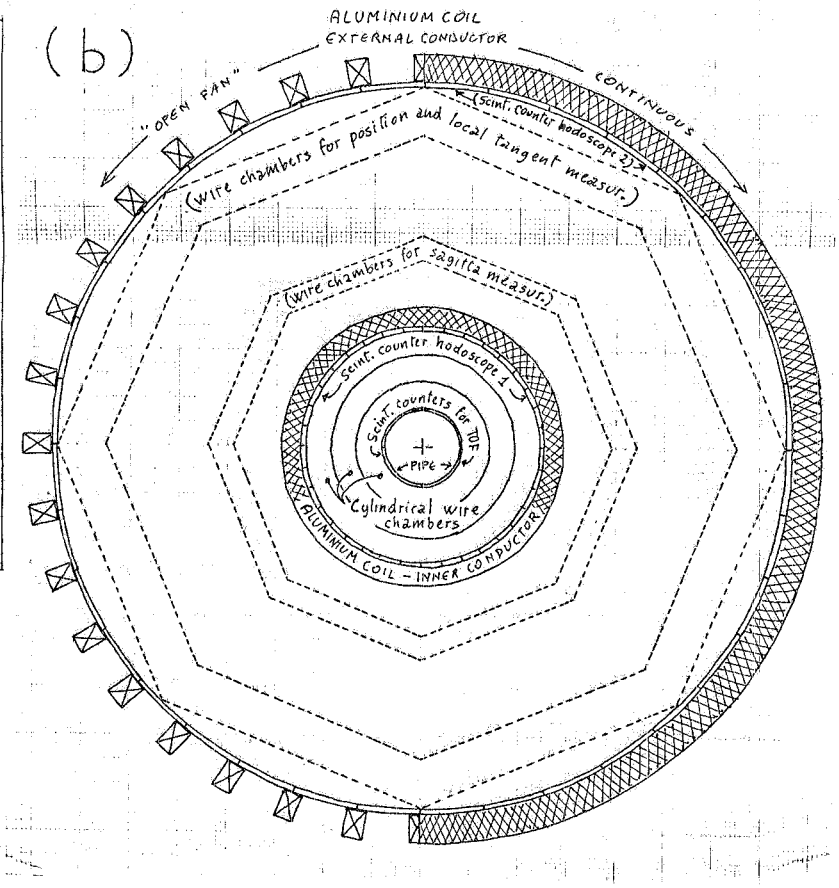

FIG. 13 - Longitudinal and transversal cross sections of the usual Aluminium coil and its detection system.

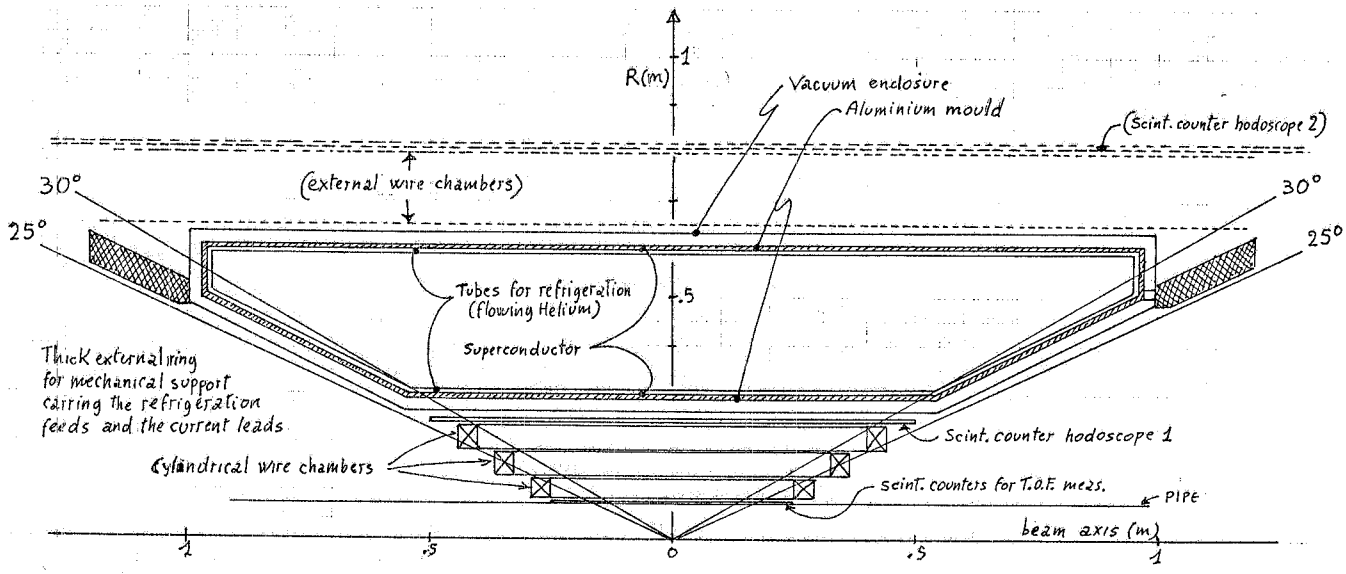

SUPERCONDUCTING TOROIDAL COIL

Overall dimension :	Length	2.4 m
	Max. Radius	0.64 m
	Min. Radius	0.26 m
Solid angle fraction ($\Delta\Omega/4\pi$)		0.87 m
Max. Magnetic Field in s.c. (at R = 0.30 m)		25.2 Kgauss
Max. Pressure from Field (at R = 0.30 m)		25.3 Atm
Current density in the superconductor		5.9×10^8 Am^{-2}
Coil stored energy		0.98 MJ

Some different solutions (see below)		A1	A2	M1	M2
Total Thickness (inner + outer)	g/cm^2	10	13	7	8
	r.l.	0.4	0.5	0.3	0.4
	L_{abs}	0.09	0.11	0.05	0.08
Momentum resolution at p = 5 GeV/c	$\theta = 90^\circ$	0.087	0.083	0.083	0.078
	$\theta = 30^\circ$	0.057	0.044	0.053	0.044
Weight (Kg)	Superconductor	260	260	260	260
	Magnet Cold Mass	510	510	390	390
	Total	700	880	480	580

A1 : Solution with the inner and the outer conductors are in one same vacuum tank.

A2 : Inner and outer conductors in two distinct vacuum tanks, to insert detectors (chambers, Cerenkovs,..) inside the magnetic volume.

M1 (M2) : The same as A1 (A2), with the Aluminum replaced by Magnesium in all the structures.

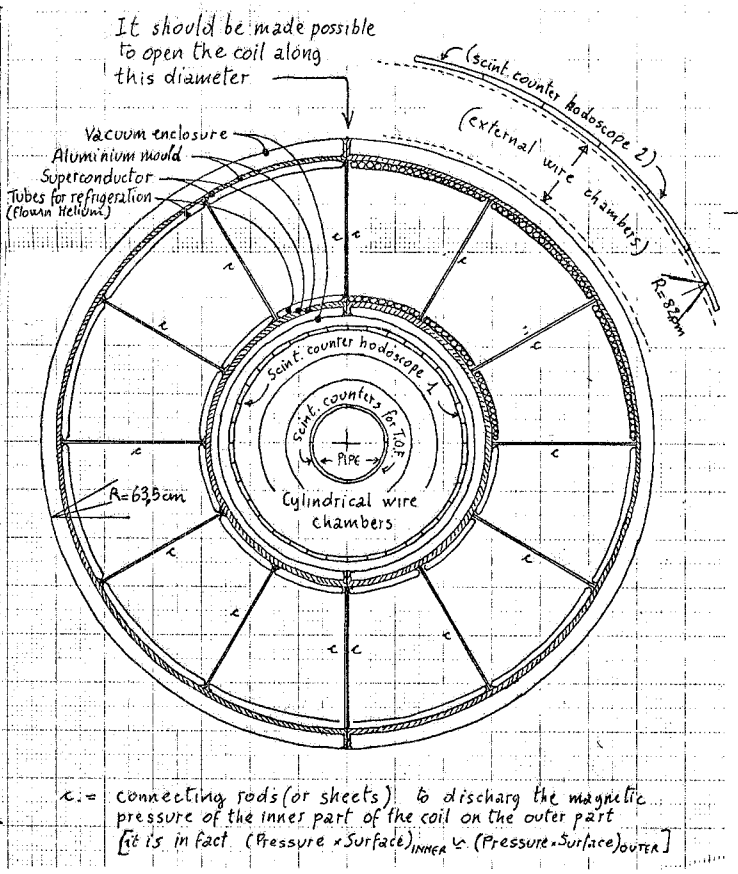

FIG. 14 - Longitudinal and transversal cross sections of the superconducting toroidal coil and its detection equipment. The drawings refer to the solution with one simple vacuum tank (solution A1 in the enclosed table).

pattern of ∿ 50% of the events and would cause ∿ 10% of any trigger hadron to be lost. It is clear that, as long as an aluminium water-cooled coil is used, it is not convenient to increase the thickness of the inner conductor, since the frequency of the inelastic interactions increases fast with it while the momentum resolution does not improve significantly.

Limiting resolution: a superconducting coil. -

A superconducting coil requires a vacuum tank and a support structure, and it can be advantageous only if the current density can be pushed very high and the ratio superconductor/cupper can be made large. The best solution is to base the coil design on the parameters of the thin solenoids constructed at LBL to test the dynamical stabilization method of operation[7]. As a reference, the coil suggested for PETRA in ref. (6) is reproduced in Fig. 14, and the momentum resolution that can be obtained is given in Fig. 15.

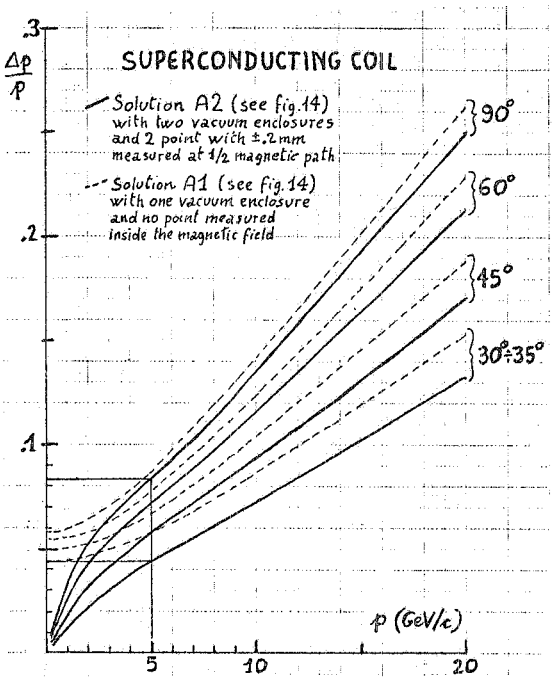

FIG. 15 - Momentum resolutions for the A1 and A2 solutions of the superconducting coil reported in Fig. 14. The momentum resolution for the M1 and M2 solution (Aluminium replaced by Magnesium) are better by a factor of 0.87 ÷ 0.97.

We consider here a possible structure of such a coil as reported in Fig. 16. Two points must be mentioned that could make this coil easier to be constructed than the test LBL coil:

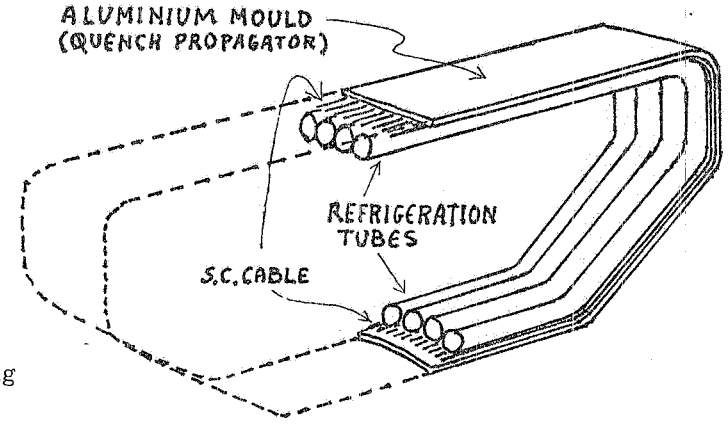

FIG. 16 - One turn of the superconducting toroidal coil.

1) As the field is $\propto 1/R$ the energy density is $\propto 1/R^2$, and is maximum where the volume is minimum, so that the stored energy is much less than in a solenoid, with the same bending power.
2) The coil works always under compression on the quenching structure, this ensuring mechanical stability and a good thermic contact.

ACKNOWLEDGEMENTS. -

I wish to express my gratitude to Prof. G. Bellettini for the usefull discussions which have been fundamental to the ideas treated in this report.

REFERENCES. -

(1) - An experiment of this type is, for instance, R 108 at the ISR (CERN-Columbia-Oxford-Rockfeller Collaboration), CERN/ISRC 73-13 (1973) and 74-54 (1974).
(2) - D. Linglin and A. Norton, Event simulation, CERN-$p\bar{p}$ note 17 (1977).
(3) - C. Mencuccini et al. in "INFN-LNF SUPERADONE Design Study" (1974), pag. 146; P. Spillantini in "Proceedings of the 1973 Intern. Conf. on Instrumentation for High Energy Physics", Frascati (1973), pag. 679; G. Bellettini and P. Spillantini, The 4π detector for the ISR Physics after 1980, Contribution to the "Workshop on Future ISR Physics", CERN (1976).
(4) - Aachen-CERN-Harvard-Munich-Riverside Collaboration, CERN/ISRC 75-33 (1975).
(5) - H. J. Besch and U. Trinks, "Vorschlang fuer linen magnetischen detektor am DESY-Speicherring", DESY Internal Report PIB 1-150 (1971).
(6) - G. Bologna et al., "A possible compact core for e^+e^- experiments", Frascati Report LNF-76/17 (1976), and "Proceedings of Discussion Meeting on PETRA Experiments, Frascati (1976).
(7) - M. A. Green et al., LBL 4611 (1975) and PEP Summer Study (1975); see also W. T. Toner, "Proceedings of Discussion Meeting on PETRA Experiments", Frascati (1976).

APPENDIX - Design of a toroidal coil for ADONE and ALA[x] ($\sqrt{s} \approx 1 \div 3$ GeV).

In multibody production at moderate total energy (as at ADONE and ALA, $\sqrt{s} \approx 1 - 3$ GeV) there is hardly any jet, it structure possible, all particles are bound to have low momentum and cannot easily be grouped into jets. A low magnetic field is sufficient to analyze any charged secondary, and the main problem for a spectrometer employing a toroidal coil is the construction of an inner conductor thin enough that a large fraction of the secondaries be absorbed in front of the spectrometer.

In the following the guide lines for the detailed project of an aluminium water-cooled thin toroidal coil for the central region at these low energies are given, having the same geometry as sketched in Fig. 10 except for the thickness of the inner conductor. Indeed, this can be reduced to only 3 mm, while being still sufficient to resist the magnetic pressure when supplied with up to 2 MW (see footnote 4) power consumption (see again Fig. 8, with $\sim$1 MW/m dissipation in the inner conductor). In this coil only a few percents of the π's produced in the most frequent interactions are absorbed by range (see Fig. 17).

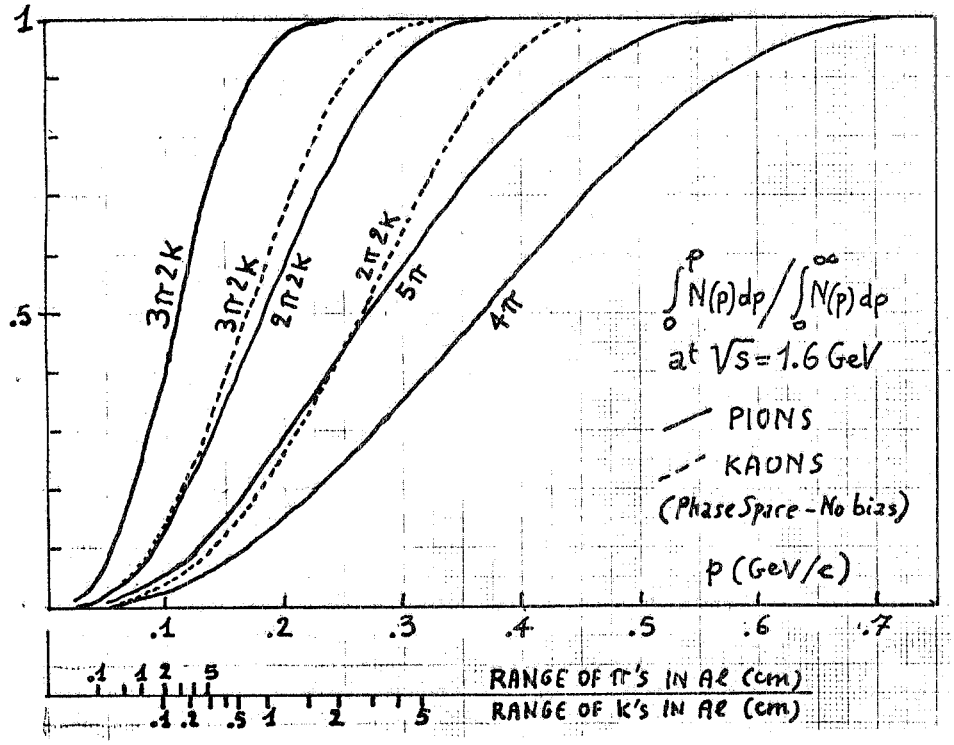

FIG. 17 - Phase space unbiased momentum distribution of π's and K's in e^+e^- annihilation at $\langle s \rangle$ = 1.6 GeV for some typical final states.

The following relations are valid:

$P = \varrho \delta^2 V$

P = dissipated power (W),
ϱ = aluminium specific conductivity = 2.83×10^{-8} $\Omega \times m$,
δ = current density (A/m^2),
V = volume of conductor.

(x) ALA is a new high intensity e^+e^- ring of energy similar to Adone, which is planned in Frascati.

Note 4 - I note that the 2 MW power supply (5000 A at 400 V) presently installed at ADONE would be adeguate for this purpose.

$I = \delta \times$ section — I = total current (A, if section in m^2) = iN,
i = current in one turn of the coil,
N = number of turns of the coil.

$p_i = P_i/N$ — p_i = power dissipated in the inner conductor by a single turn (W),
P_i = power dissipated in the whole inner conductor.

$q_i = c\, m_i \Delta T$ — q_i = as p_i, but measured in cal/sec = $P_i/4.18$,
m_i = water flowing per second in a single turn in the inner conductor (gr/sec),
ΔT = temperature variation of the water (^oC) from input to output,
c = specific heat of the water ($\simeq 1$ cal/gr.^oC).

$$P_W = 0.0025\, l_i \frac{(\frac{M_i}{n})^2}{d^5}$$

P_W = pressure of the water (m of water/cm^2),
l_i = length of the inner conductor (m),
M_i = as m_i, but measured in m^3/sec $\simeq 10^{-6}\, m_i$,
n = number of water leads (circular and identical) in each coil in the inner conductor,
d = diameter of the hole (m).

$$R_W = \frac{Nn\pi(d/2)^2}{2\, R_i x \langle s \rangle}$$

R_W = ratio between the sections of the cooling water cricuit and of the aluminium in the inner conductor,
$\langle s \rangle$ = average thickness of the aluminium in the inner conductor (m),
R_i = internal radius of the coil (m).

$x = 10^{-4} p_i/n\pi d l_i$ — x = power exchanged between the aluminium and the water in each leads in the inner conductor (W/cm^2).

These formulae when applied to the coil of Fig. 10 with $\langle s \rangle$ as a parameter (and assuming the section of the aluminium conductor in the lateral and external sections of the coil to be five times larger than in the inner conductor), give:

$$P_{TOTAL} = \varrho\,(\delta_i^2 V_i^2 + \delta_e^2 V_e^2) = P_i + P_{REST},$$

where:

P_{TOTAL} = power dissipated in the whole coil = 2 MW (see Footnote 4),
P_i = power dissipated in the inner conductor,
P_{REST} = power dissipated in the lateral and external conductors.
δ_i = current density in the inner conductor,
δ_e = current density in the lateral and external conductors = $0.2\, \delta_i$,

hence for the inner part of the coil we have:

$$P_i = \frac{1}{1.569} P_{TOT} = 1.275 \times 10^6 \text{ W} \rightarrow \frac{P_i}{l_i} = 0.98 \times 10^6 \text{ W/m}$$

$$\delta = 4.70 \times 10^6 \frac{1}{\sqrt{\langle s \rangle}} \text{ A/m}^2$$

$$I = 7.38 \times 10^6 \sqrt{\langle s \rangle} \text{ A}$$

$$N = \text{INTEGER}\,(1.48 \times 10^3 \times \sqrt{\langle s \rangle})$$

$$p_i = 862 \frac{1}{\sqrt{\langle s \rangle}} = 4.18 \times 10^6 M_i \Delta T = 4.08 \times 10^4\, n \times d$$

$$d = 0.0367 \times \sqrt{R_W/n} \times \sqrt[4]{\langle s \rangle}$$

$$x = 0.575/(\sqrt{n \times R_W} \times \sqrt[4]{\langle s \rangle})$$

$$P_W = 0.0025\, l_i \frac{(M_i/n^2)}{d^5} = 0.312 \times 10^{-6} \frac{x^2}{\Delta T^2} \frac{1}{d^3} .$$

Numerical values for two average aluminium thickness $\langle s \rangle$ are reported in Table II.

TABLE II

$\langle s \rangle$ (m)	δ (A/m^2)	I (A)	N	Width of one current turn $\lambda = 2\pi R_i/N$ (m)	P_i (W)	M_i for $\Delta T = 30^\circ C$ (m^3/sec)	for $R_W = 0.25$					
							water velocity (m/sec)	n = 1		n = 2		n = 4	
								d (m)	P_W (Atm)	d (m)	P_W (Atm)	d (m)	P_W (Atm)
0.003	86.0×10^6	404×10^3	81	0.0194	15.75×10^3	0.126×10^{-3}	9.18	0.0093	4.6	0.0030	6.5	0.0021	9.2
0.005	66.6×10^6	524×10^3	104	0.0151	15.25×10^3	0.098×10^{-3}	4.22	0.0055	0.75	0.0039	1.06	0.0027	1.5

The last formula can be represented in a graph (see Fig. 18) in the form:

$$d = \frac{0.68 \times 10^{-2}}{\sqrt[3]{P_W}} \sqrt[3]{\left(\frac{x}{\Delta T}\right)^2} .$$

This graph helps in finding easily the working point for the inner part of the coil (pressure and temperature gradient of the water, and amount of heat exchanged between the aluminium and the water). Numerically, for $R_W = 0.25$ and $P_W = 80$ m of water/cm^2 $\simeq$ 8 Atm we obtain:

$\langle s \rangle = 0.003$ m	n = 1	x = 96 W/cm^2	d = 4.2 mm	$\Delta T = 22^\circ C$
	n = 2	68 W/cm^2	3.0 mm	$26^\circ C$
	n = 4	48 W/cm^2	2.1 mm	$31^\circ C$
	n = 8	34 W/cm^2	1.5 mm	$38^\circ C$
$\langle s \rangle = 0.005$ m	n = 1	68 W/cm^2	6.0 mm	$9^\circ C$
	n = 2	48 W/cm^2	4.2 mm	$11^\circ C$
	n = 4	34 W/cm^2	3.0 mm	$14^\circ C$
	n = 8	24 W/cm^2	2.0 mm	$18^\circ C$

Values of x and ΔT are technically accessible already for $\langle s \rangle = 0.003$ m and $n \leq 8$. The choice of n depends on the design of the section of the conductor.

The assumed value for $R_W (\sim 0.25)$, the convenience of chosing a simple shape (rectangular) for the section of the conductor, and the need of a safe thickness of aluminium around the lead

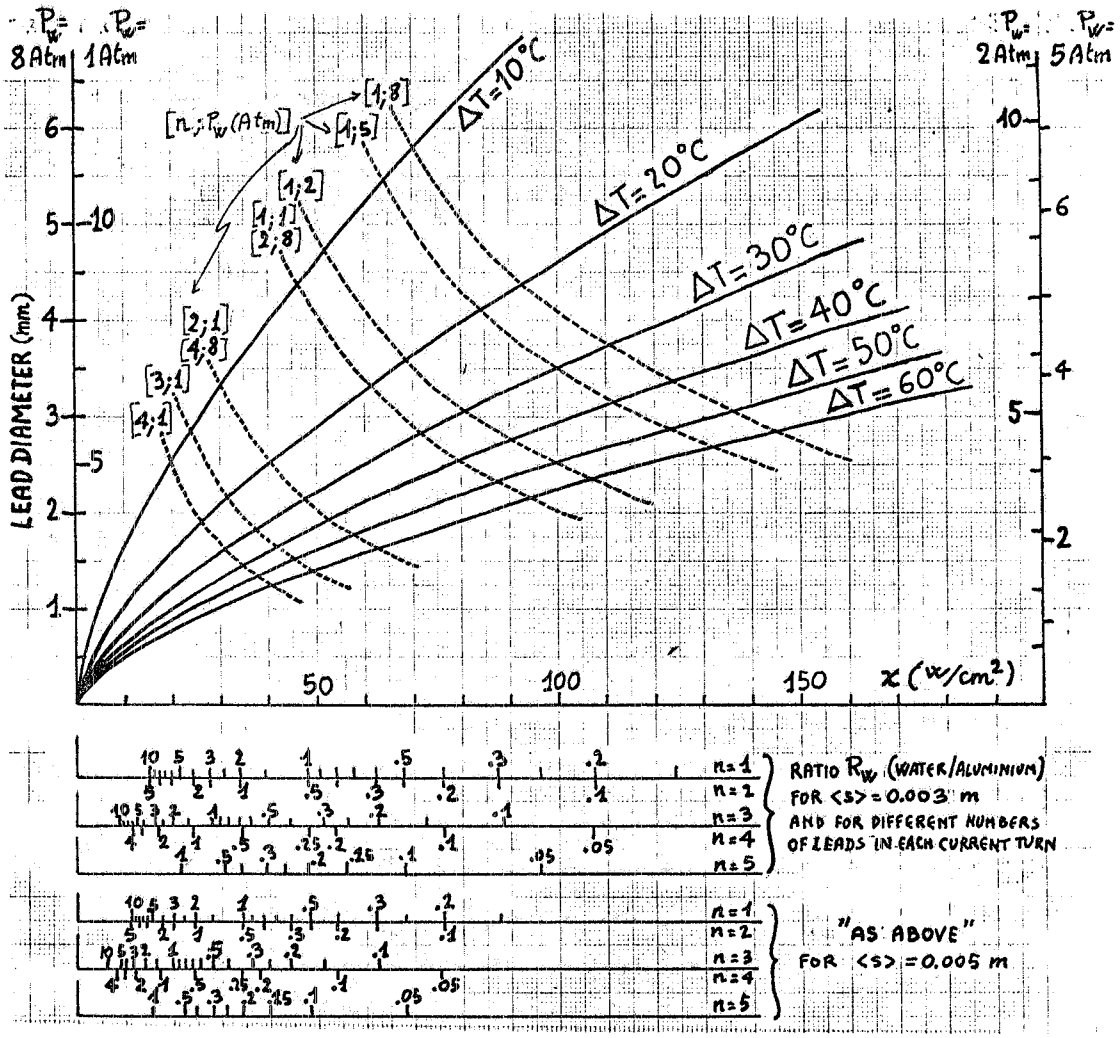

FIG. 18 - Lead diameter (d in mm) versus power (x in W/cm^2) exchanged between the aluminium and the water in each lead in the inner portion of the coil, for different temperature gradients (ΔT) of the water (solid lines) and for different numbers of leads per current turn (n) and different water pressures (P_W inAtm) (broken lines). Different ordinate scales refer to different values of the water pressure P_W. The additional scales in abscissa refer to the values of the ratio (R_W) between the sections of the cooling water circuit and the aluminium in the inner portion of the coil, for different thickness $\langle s \rangle$ of the conductor in the inner portion of the coil and different values of n.

($\gtrsim 0.8$ mm) imposes $n \geq 4.1$ (see footnote 5). Assuming n = 5, with slight corrections to the numbers we obtain for the coil the final parameters reported in Table III.

One current turn in the inner portion of the coil comprises 5 conductors in parallel each 4 mm x 4 mm in section with a hole 2.4 mm in diameter (see Fig. 19). On the sides and radially outwards the coil is made out the parallel of 25 such conductors (see Fig. 20). The working point for the heath exchange mechanism in the inner portion of the coil is :

Note 5 - For a rectangular shape ($\langle s \rangle \times \lambda$ in section) of the current turn we have the condition $n \geq \frac{4R_W}{d^2} \cdot \frac{\langle s \rangle \lambda}{\pi}$ with $d = \langle s \rangle + R_W \langle s \rangle - 2t$ (t = minimum thickness of the aluminium around the hole).

TABLE III

Main parameters of the toroidal coil for the low momentum region.

Overall dimensions :	Length	2 m	
	Max. Radius	1 m	
	Min. Radius (R_i)	0.254 m	(Slightly corrected from the value (0.25 m) quoted in Table I)
Solid angle ($\Delta\Omega/4\pi$)		0.91	
Number of current turns		80	(it was 81 in Table II)
Section of each current turn			
in the inner conductor		4×20 mm^2	(it was 3.75×19.4 in Table II)
in the side and outer conductors		20×20 mm^2	
Number of leads for the cooling water in each turn in the inner conductor		5	
Diameter of the leads		2.4 mm	
R_W		0.23	(originally assumed 0.25)
Average thickness of the inner cond.		3.25 mm	(originally assumed 3.0 in Table II)
Total weight		285 Kg	(compare with 360 in Table I)
If supplied with a 2 MW power, we have :			
Max. magnetic field (at R = 0.25 m)		0.32 T	(compare with 0.65 in Table II)
Max. magnetic pressure (at R=0.25 m)		0.40 Atm	(1.65 in Table I)
Current density			
in the inner conductor		77 A/mm^2	(52 in Table I)
in the side and outer cond.		15.4 A/mm^2	
Momentum resolution at p = 1 GeV/c (Device as in Fig. 10, with the same precisions)	(90°)	0.064	(0.051 in Fig. 11)
	(40°)	0.031	(0.021 in Fig. 11)

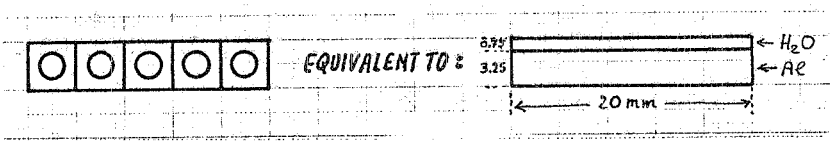

FIG. 19

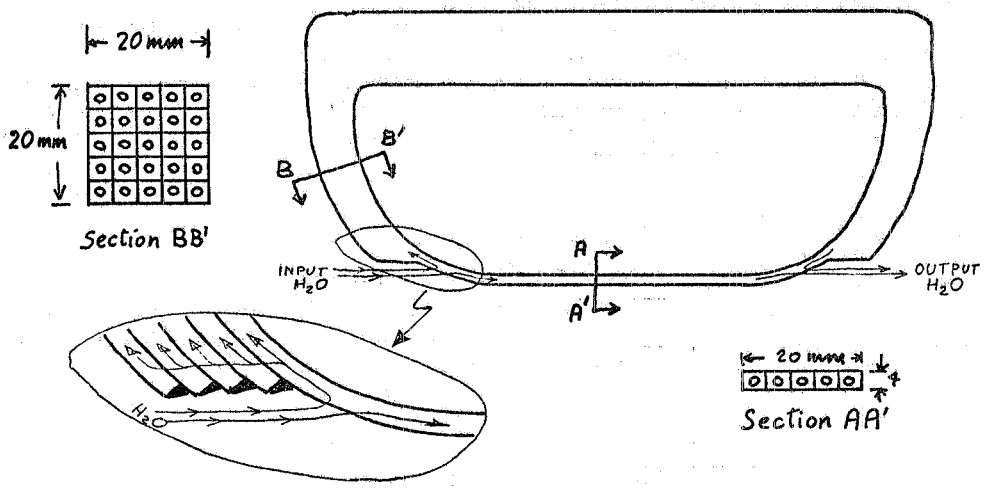

FIG. 20 - One current turn of the toroidal coil (Schematic, not in scale)

$x = 42\ W/cm^2$ $\quad \Delta T = 28^{\circ}C$ at $P_W = 5$ Atm ,

$x = 42\ W/cm^2$ $\quad \Delta T = 22^{\circ}C$ at $P_W = 8$ Atm ,

$x = 42\ W/cm^2$ $\quad \Delta T = 17^{\circ}C$ at $P_W = 16$ Atm.

In the external part of the coil the current turns can be collected 5 by 5 in 16 rods composed of 125 conductors of $4 \times 4\ mm^2$ each. Rearranging the conductors in rods $10 \times 200\ mm^2$ in section, about 97% of the external surface of the toroid is completely transparent to the outgoing particles. The momentum resolution obtainable with a 2 MW power supply (assuming for the detection system the same dimensions and performances as in Fig. 10 and 11) is given in Fig. 21.

Although the described coil gives, for the same power, a field which is $\sim$1.7 times weaker the the one produced by the coil sketched in Fig. 10, the corresponding momentum resolution for $p \lesssim 3$ GeV/c is worse by only 20÷40 % (This is because the multiple scattering in the inner conductor (reduced from 10 to 3.25 mm) gives now a much smaller contribution to the total error in momentum measurement).

In Fig. 22 this momentum resolution is combined with that forseen for an U-compensated hadron calorimeter (around $0.25/\sqrt{p}$), to show how effective this light toroid could be if used as central "pattern recognition device" in a complex apparatus.

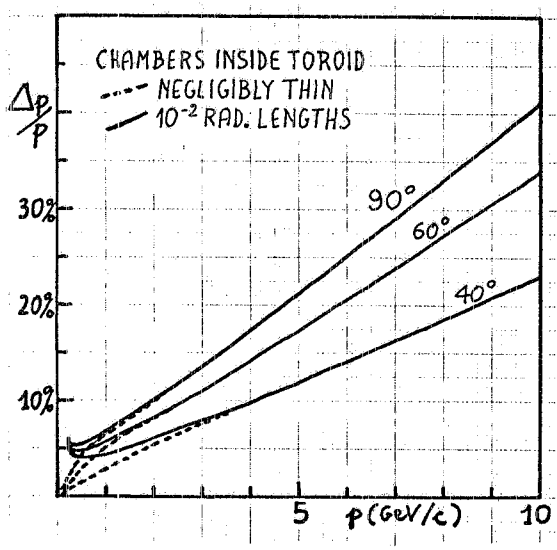

FIG. 21

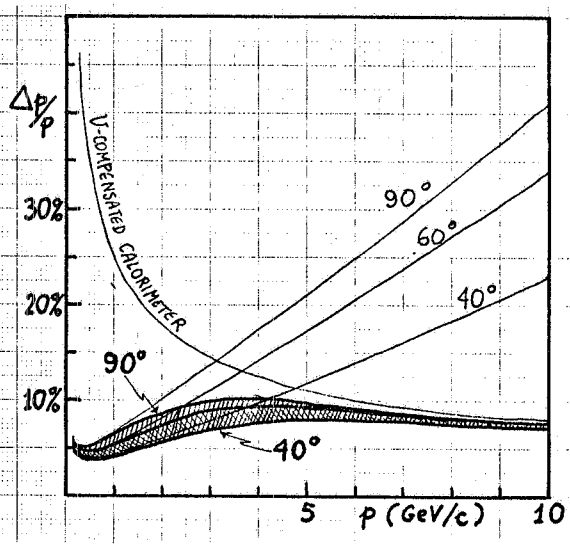

FIG. 22